XLIII CILAMCE
21–25, November, 2022
FOZ DO IGUAÇU – PR – BRAZIL

# Numerical analysis of structures with a GFRP application in a transmission line tower

Leonardo W. Felchak[1], Kelvin L. Becker[1], Ana C. A. Lopes[2], Joseane V. Gulmine[1], Renan M. O. Pereira[1]

[1] *Segmento de Pesquisa, Desenvolvimento e Inovação, Lactec,*
*PO Box 19.067, CEP 81531-980, Curitiba - PR, Brazil,*
*renan.pereira@lactec.org.br, leonardo.felchak@lactec.org.br, kelvin.becker@lactec.org.br,*
*joseane.gulmine@lactec.org.br;*
[2] *Copel Geração e Transmissão, S. A.*
*Rua José Izidoro Biazetto nº 158, CEP 81200-240, Curitiba – PR, Brazil,*
*ana.aoki@copel.com.*

**Abstract.** This work aims to investigate through numerical simulations the mechanical behavior of the glass fiber reinforced polymeric (GFRP) line post structures. It is presented a numerical validation of the mechanical properties of the composite material, in order to ensure the representativeness of the model. Additionally, in order to understand the impact of parameters change, such as fibers orientation, layer thickness, and resin type in the structure model, the structure mechanical response curves is evaluated. Therefore, a parametric analysis is made to provide an understanding on the structure response characteristics such as load *versus* displacement, stress *versus* deformation, buckling modes, as well as the cause and effect relationship in the results obtained. The orientation of the fibers showed to be the most important parameter on the mechanical behavior of the structure, as well as the number of layers, a factor observed as being one of the most relevant in the verifications of the buckling modes.

**Keywords:** transmission line poles, glass fiber reinforced polymer, numerical modeling, finite element method.

## 1 Introduction

The transport of electric energy from generating plants to distribution centers and to consumers is carried out by transmission towers. These structures have the function of supporting the weight of transmission line cables, as well as the weather conditions on it. Usually, these towers are made of steel, which requires frequent maintenance, and are highly susceptible to corrosion and vandalism, which requires emergency towers replacement.

Marzuki and Jaafar [1] evaluated the mechanical strength and reserve factor of samples of glass fiber reinforced polymers (GFRP) through simulations with CompositeStar© software. The composite panels were varied in terms of fiber direction and the authors shown that bidirectional and quasi-directional fiber orientation have balanced strength and an acceptable reserve factor in both directions.

Urgessa and Mohamadi [2] presented a finite element analysis of fiber-reinforced polymer composite poles. The study involved a parametric evaluation of geometric characteristics, fiber orientation, number of layers and lamina thickness. The authors founded that a maximum stress increase occurs when fiber-orientation increases up to 45° with respect to the axial direction, and a decrease is verified when fiber-orientation increases up to 60°.

Santos and Junior [3] studied monocoque and semi-monocoque GRFP poles configurations, using longitudinal stiffeners and transverse rings, in different combinations. Finite difference method was employed in determination of the maximum pole end deflection, and a structural stability and failure analysis was also conducted in commercial software Abaqus™. The author verified that the addition of stringers and rings resulted in an increase in buckling critical load, and the occurrence of local buckling near the base, also a maximum deflection was noted in the regions of the stringers.

This work presents part of the results of the R&D project PD-06491-0481/2018 "DESENVOLVIMENTO

DE COMPÓSITOS POLIMÉRICOS PARA CONSTRUÇÃO DE TORRES USADAS EM LINHAS DE TRANSMISSÃO " developed by Lactec for Copel Geração e Transmissão S.A. within the scope of the Programa de Pesquisa e Desenvolvimento Tecnológico do Setor Elétrico regulamentado pela Agência Nacional de energia Elétrica (ANEEL). The study aims to evaluate the application of power transmission poles, manufactured by the filament winding process, built with GFRP. The GFRP is a composite material that has properties such as lightness, lower cost compared to steel, in addition to streamlined construction, desirable characteristics especially in places of difficult access, like the frequently found in transmission line towers location spots. The study proposes to analyze the mechanical performance of GFRP structures via computer simulation with the finite element method (FEM), making it possible to infer predictions of the structural behavior of this type of material for post applications in line post structures (individual), in addition to observing differences between the mechanical response of both applications.

In this study, the simulations were carried with the use of the finite element method (FEM), considering the geometric non-linearity, and the orthotropy of the composite material. The mechanical properties were obtained experimentally by laboratory tests carried out at LACTEC. Loads and displacement restrictions usually considered in the structural calculation of the posts were applied as boundary conditions of the model. Different configurations of resin types, composite thickness, number of layers, and fiber orientation were evaluated with the assistance of parameterization of numerical modeling aspects, aiming to understand the influence of different parameters of the pole manufacturing process on the structural performance of the final product. The finite element analysis performed in this work provided a clear understanding of the trade-off relations between the parameters, and also issued a sensibility analysis of those design variables.

## 2 Experimental studies

The flexural test was performed according to ASTM 790 – 2017 – Flexural Properties of Unreinforced and Reinforced Plastics and Electrical Insulating Materials [4]. In this test, rectangular specimens were positioned under support with two fixed points and a movable central point responsible for applying the load at a constant speed. A universal testing machine from the manufacturer Instron, model 33R4467, with a load cell of 1 kN, was employed to perform the test. The test arrangement is show in Figure 1.

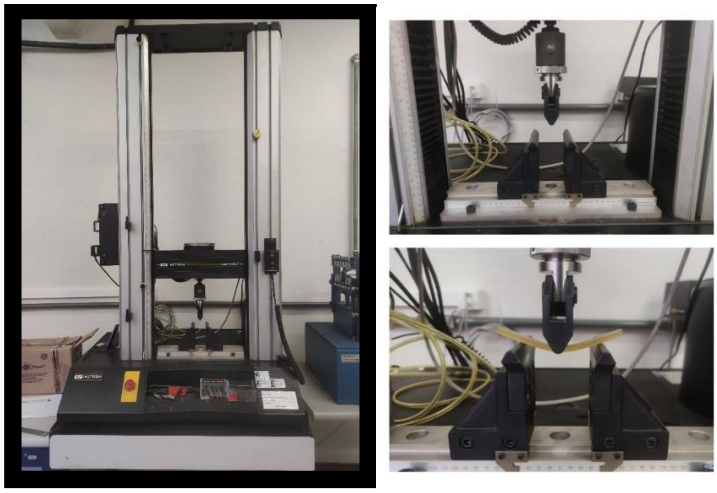

Figure 1. ASTM 790 flexural test arrangement

During the test, the values of load ($F$) and deflection are recorded. Knowing the dimensions of the specimens, width ($l$), and thickness (v), it is possible to obtain the bending stress ($\sigma_f$) through the following equation:

$$\sigma_f = \frac{3FL}{2ld^2} \tag{1}$$

The flexural modulus is obtained by evaluating the stress x strain curve, through the variation of stress by the variation of strain in the linear region.

# 3 Numerical modeling procedures

Two geometry configurations are presented for the line post structure, as Table 1 shows. The first structure configuration has 30 meters of height, 570 mm diameter in the bottom and 280 mm in the top, with 3.6 m of grounding. The second configuration presents a height of 20 meters and 750mm and 500mm for the diameters of the bottom and the top respectively, with 2.6 m of grounding. The grounding length is a manufacturer recommendation of 10% of the total pole length plus 0,6 m to be clamped in the ground.

The model element size is set to 50mm according to the convergence test, which resulted in 15025 nodes and 15000 elements for the C1 post, while for the C2 post the mesh statistics were 15238 nodes and 15200 elements for the C2 post. The post skin was modelled as SHELL281 elements, which are suitable for analyzing thin to moderately-thick shell structures. This element has eight nodes with six degrees of freedom at each node, it accounts for linear, large rotation and/or large strain nonlinearities. Figure 2 shows the finite element mesh for the C1 line post model and Figure 3 shows the mesh for the C2 line post model. Table 1 summarizes the FEM model data.

Table 1. Finite element model geometry and mesh data

| Structure | Diameter of the base (mm) | Diameter of the top (mm) | Length (m) | Grounding (m) | Number of elements | Number of nodes |
|---|---|---|---|---|---|---|
| C1 Pole | 570 | 280 | 30 | 3.6 | 15000 | 15025 |
| C2 Pole | 750 | 500 | 20 | 2.6 | 15200 | 15238 |

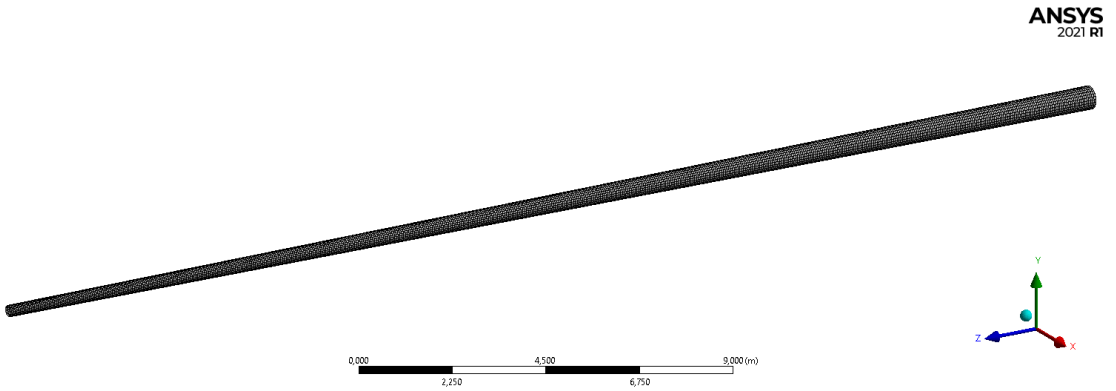


Figure 2. Finite element mesh of the C1 line post

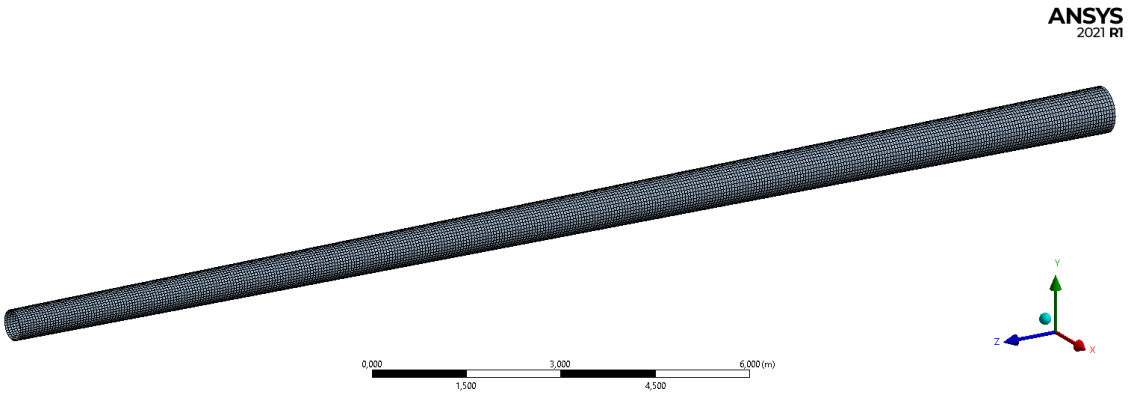


Figure 3. Finite element mesh of the C2 line post

A finite element analysis based on classic laminate theory (CLT) was conducted on ANSYS ACP software, as the CLT basic assumptions are fulfilled in a relatively thin or moderate thick laminate where the thickness is small compared to the in-plane extensions (length and width), which is the case for the pole geometries.

The numerical analysis was defined on non-symmetric GFRP layup, in which several fiber orientation and layer thickness were evaluated. Table 2 shows the orthotropic elastic material properties for three different GFRP composite resins matrix. The resin A is a bicomponent epoxy resin. On the other hand, the B and C resins are composed by unsaturated polyester base. Table 3 presents the fabrics and layup properties assessed for the study. The composite has a 70% fiber and 30% resin proportion. For all the GFRP a 2,17 g/cm³ density was considered, this was obtained based on the fiber/resin proportion, considering the glass fiber density of 2,6 g/cm³ and that the resins density is around half of the fibers.

The orthotropic material properties were defined based on three-point bending test results. The Young's modulus in fiber direction was assumed to be equal to the flexural modulus for longitudinal fiber and the Young's modulus in other directions were assumed as equal to the flexural modulus obtained for transversal fiber. In cases where composites specimens were tested at fiber orientations of 30 or 60 degrees, the flexural modulus for longitudinal and transversal fiber orientations were obtained by linear interpolation.

The shear modulus was obtained from the following equation:

$$G_{xy} = \frac{E_1 E_2}{E_1 + E_2 + 2E_2 v_{12}}, G_{23} = G_{13} = G_{12} \tag{2}$$

where:

$E_1$ = Young modulus in fiber direction (MPa);

$E_2$ = Young modulus orthogonal to fiber direction (MPa);

$v_{12}$ = Poisson ratio at the layer plane;

$G_{12}$ = Shear modulus at the layer plane (MPa);

$G_{13}$ = Shear modulus at the layer plane in fiber direction (MPa);

$G_{23}$ = Shear modulus out of the layer plane normal to fiber direction (MPa).

Table 2. Material Engineering Constants

| Mechanical Properties | Symbol | GFRP (resin A) | GFRP (resin B) | GFRP (resin C) |
|---|---|---|---|---|
| Young Modulus in Fiber Direction (MPa) | $E_1$ | 14000.00 | 7100.00 | 22635.20 |
| Young Modulus Orthogonal to Fiber Direction (MPa) | $E_2$ | 2240.00 | 8300.00 | 3020.00 |
| Young Modulus Out-of-Plane Direction (MPa) | $E_3$ | 2240.00 | 8300.00 | 3020.00 |
| Poisson Ratio at the Layer Plane | $v_{12}$ | 0.16 | 0.16 | 0.16 |
| Poisson Ratio Out of the Layer Plane in Fiber Direction | $v_{13}$ | 0.16 | 0.16 | 0.16 |
| Poisson Ratio Out of the Layer Plane Orthogonal to Fiber Direction | $v_{23}$ | 0.16 | 0.16 | 0.16 |
| Shear Modulus at the Layer Plane (MPa) | $G_{12}$ | 1849.41 | 3263.74 | 2567.78 |
| Shear Modulus at the Layer Plane in Fiber Direction (MPa) | $G_{13}$ | 1849.41 | 3263.74 | 2567.78 |
| Shear Modulus Out of the Layer Plane Normal to Fiber Direction (MPa) | $G_{23}$ | 1849.41 | 3263.74 | 2567.78 |

The layered composite shell properties such as number of layers, fiber orientation, resin type and layer thickness were parametrized and automatically created the finite element models with the correspondent parameters associated. Table 3 shows all different layered composite shell model parameters assessed, each FE model was defined as a design point (DP) in the Ansys Parameter set tool.

Figure 4 illustrates the fiber angle orientation, which is referred to the mandrill axis. In the model definition every composite layer has fibers oriented at $\pm\phi$, where $\phi$ is the fiber angle to the mandrill axis.

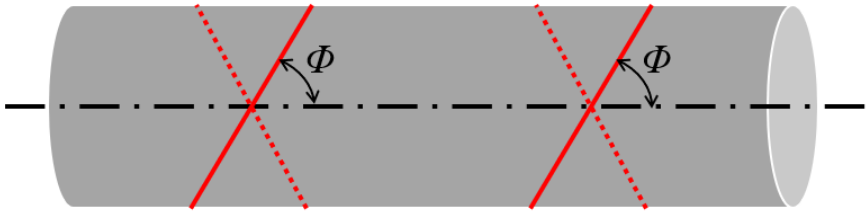


Figure 4. Fiber orientation convention

Table 3. FE Model parametrization

| Design Point | Resin type | Total thickness (mm) | Layer thickness (mm) | Number of ±60 layers | Number of ±45 layers | Number of ±30 layers |
|---|---|---|---|---|---|---|
| DP 0 | A | 20 | 0,56 | 36 | - | - |
| DP 1 | A | 40 | 0,56 | 72 | - | - |
| DP 2 | B | 20 | 0,56 | 36 | - | - |
| DP 3 | B | 40 | 0,56 | 72 | - | - |
| DP 4 | C | 20 | 0,56 | 36 | - | - |
| DP 5 | C | 40 | 0,56 | 72 | - | - |
| DP 6 | A | 20 | 0,56 | - | 36 | - |
| DP 7 | A | 40 | 0,56 | - | 72 | - |
| DP 8 | B | 20 | 0,56 | - | 36 | - |
| DP 9 | B | 40 | 0,56 | - | 72 | - |
| DP 10 | C | 20 | 0,56 | - | 36 | - |
| DP 11 | C | 40 | 0,56 | - | 72 | - |
| DP 12 | A | 20 | 0,56 | - | - | 36 |
| DP 13 | A | 40 | 0,56 | - | - | 72 |
| DP 14 | B | 20 | 0,56 | - | - | 36 |
| DP 15 | B | 40 | 0,56 | - | - | 72 |
| DP 16 | C | 20 | 0,56 | - | - | 36 |
| DP 17 | C | 40 | 0,56 | - | - | 72 |
| DP 18 | A | 20 | 0,56 | 12 | 12 | 12 |
| DP 19 | A | 40 | 0,56 | 24 | 24 | 24 |
| DP 20 | B | 20 | 0,56 | 12 | 12 | 12 |
| DP 21 | B | 40 | 0,56 | 24 | 24 | 24 |
| DP 22 | C | 20 | 0,56 | 12 | 12 | 12 |
| DP 23 | C | 40 | 0,56 | 24 | 24 | 24 |

### 3.1 Eigenvalue buckling

The analysis of the structural stability (buckling), is made with FEM. Thus, the problem of eigenvalues is solved, as shown by Equation (3), which estimates the critical buckling load of the structure ([5]).

$$([K] + \lambda_i[S])\{\psi_i\} = 0 \qquad (3)$$

where: [K] is the stiffness matrix corresponding to the base state, which includes the effects of the preloads; $\lambda_i$ is the $i^{th}$ eigenvalue; [S] is the stress stiffness matrix; $\{\psi_i\}$ is the $i^{th}$ eigenvector of displacements; i refers to the $i^{th}$ buckling mode.

The buckling problem is solved by linear perturbation analysis procedure, which involves a prior linear or nonlinear preloaded status (base analysis). The boundary conditions for the linear preloaded status selected for the stability analysis comprehends a unitary vertical load applied to the pole top edge and a fixed support attached to the clamped face of the pole. Those boundary conditions related to the preloaded status are shown in Figure 5.

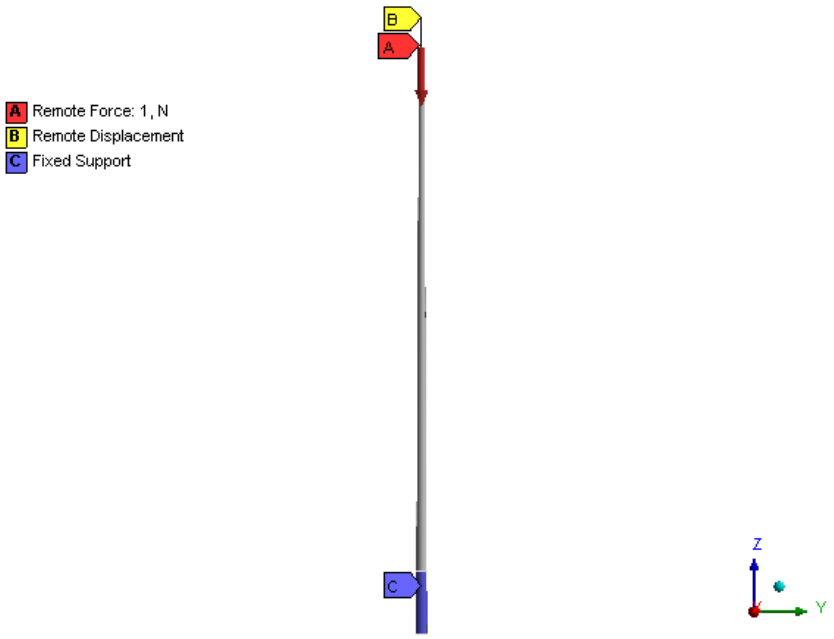


Figure 5. Preloaded status boundary conditions for eigenvalue buckling analysis

### 3.2 Static structural non-linear analysis

A geometrically non-linear analysis considering a maximum design wind load case was assessed. The typical design wind loading case load parameters and values are presented in Table 4 and Table 5.

Table 4. Load calculation parameters

| Parameter | Unit | Value |
|---|---|---|
| Weight span | m | 100.00 |
| Cable linear weight | kg/m | 1.60 |
| Wind span | m | 80.00 |
| Wind speed | m/s | 17.00 |
| Line deflection angle | º | 1.00 |
| Air density | kg/m³ | 1.23 |
| Cable diameter | mm | 26.40 |

Table 5. Load values

| Load direction | Value (N) |
|---|---|
| Vertical load | 1567.74 |
| Transverse load | 1193.39 |

Figure 6 shows the boundary conditions considered for the FE model and the real tower structure scheme, 4 concentrated loads (A, B, C, E) are applied in the structure, which represents the 4 points of cable attachment, a clamped face (F), due to the grounding part, and acceleration due to gravity (D). Each punctual load, except the wind load on structure corresponds to the forces transmitted by an insulator, and represents the resultant of the vertical and transverse components shown in Table 5. The loads transmitted by inferior conductor cables to structure crossarm were neglected for modeling.

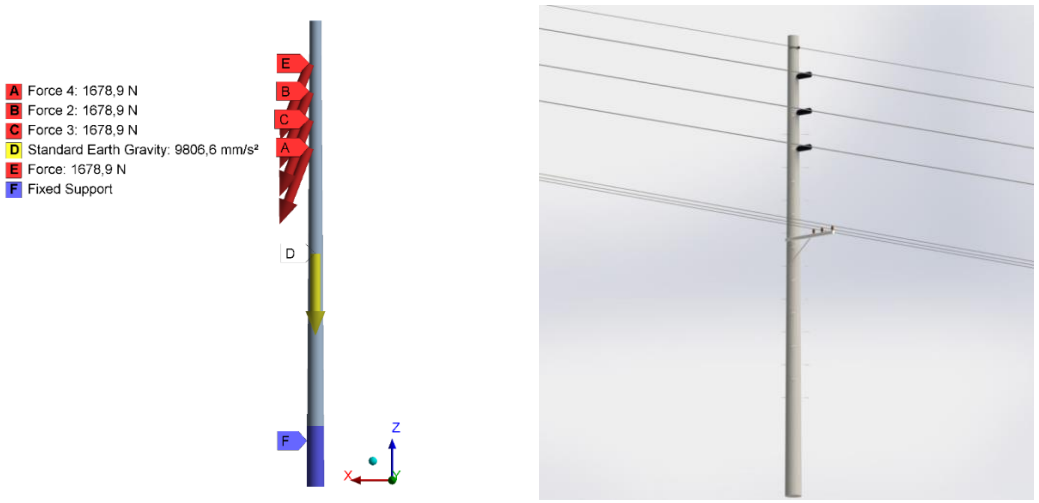


a) FE model boundary conditions b) Transmission line tower setup

Figure 6. Maximum wind load case analysis

# 4 Results and Discussions

This section presents the results of a parametric analysis, which was conducted to understand the mechanical response of GFRP structures. The properties study includes the type of resin, geometric characteristics, fiber orientation, number of layers, and lamina thickness. The finite element analysis includes the simulation of the critical buckling load, as well as the loading combination of the cable weight and wind on the cables.

## 4.1 Buckling analysis

The FEA buckling analysis is performed to discover the critical load that makes the structure stability fail under a vertical load. Critical buckling loads and mode shapes are the results from eigenvalue and eigenvectors obtained in the analysis. The first two design points eigenvectors results were very similar. It occurs due to identical boundary and analogous geometry configuration.

Figure 7 presents the first buckling modes for C1 and C2 line post, respectively. The first buckling mode shapes and critical buckling loads are approximately the same, and both present global buckling modes, differing only by the displaced direction. The critical buckling loads comparison results for all structures mentioned in Table 3 are presented in Figure 8 and Figure 9. Table 6 presents direct comparison between design points, providing a better understanding of the trade-off relationship of parameters as thickness increase, resin type and fiber orientation.

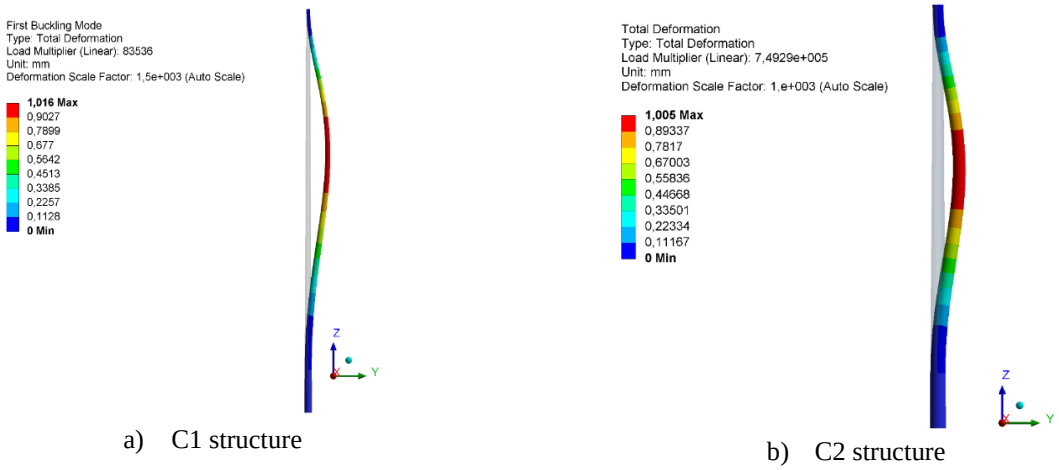


a) C1 structure b) C2 structure

Figure 7. First buckling modes for C1 and C2 structures

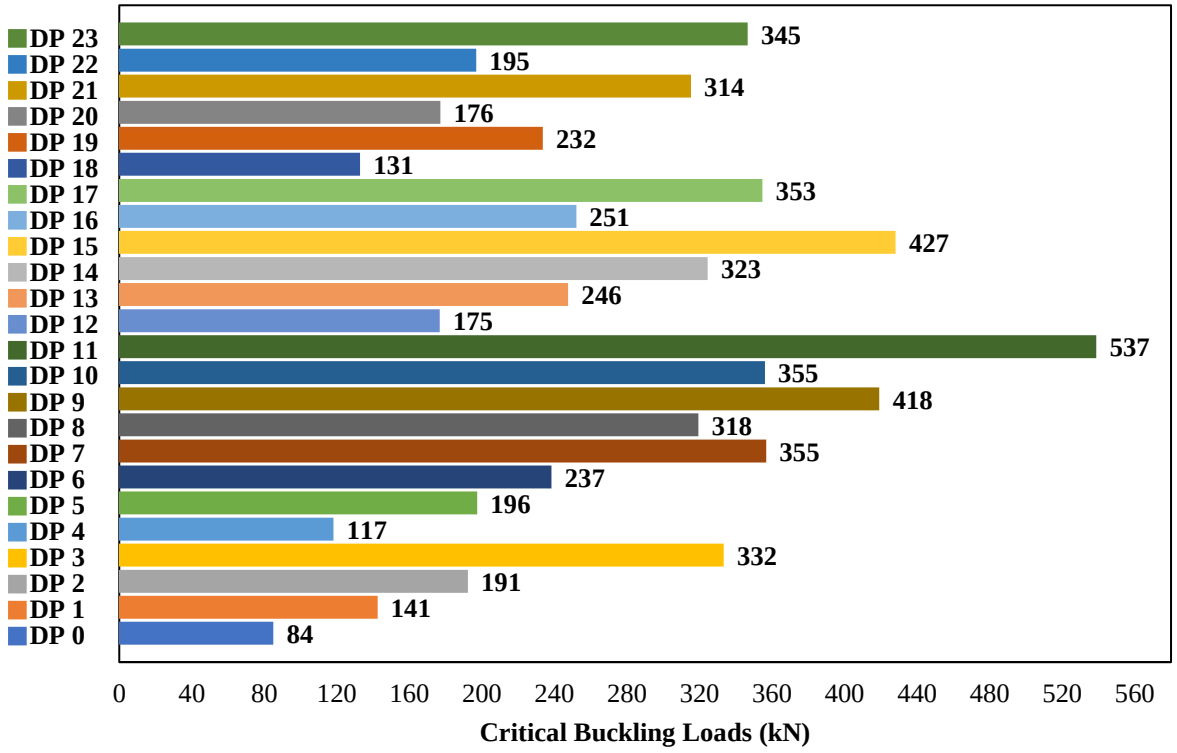


Figure 8. Two first C1 30m pole buckling mode critical loads

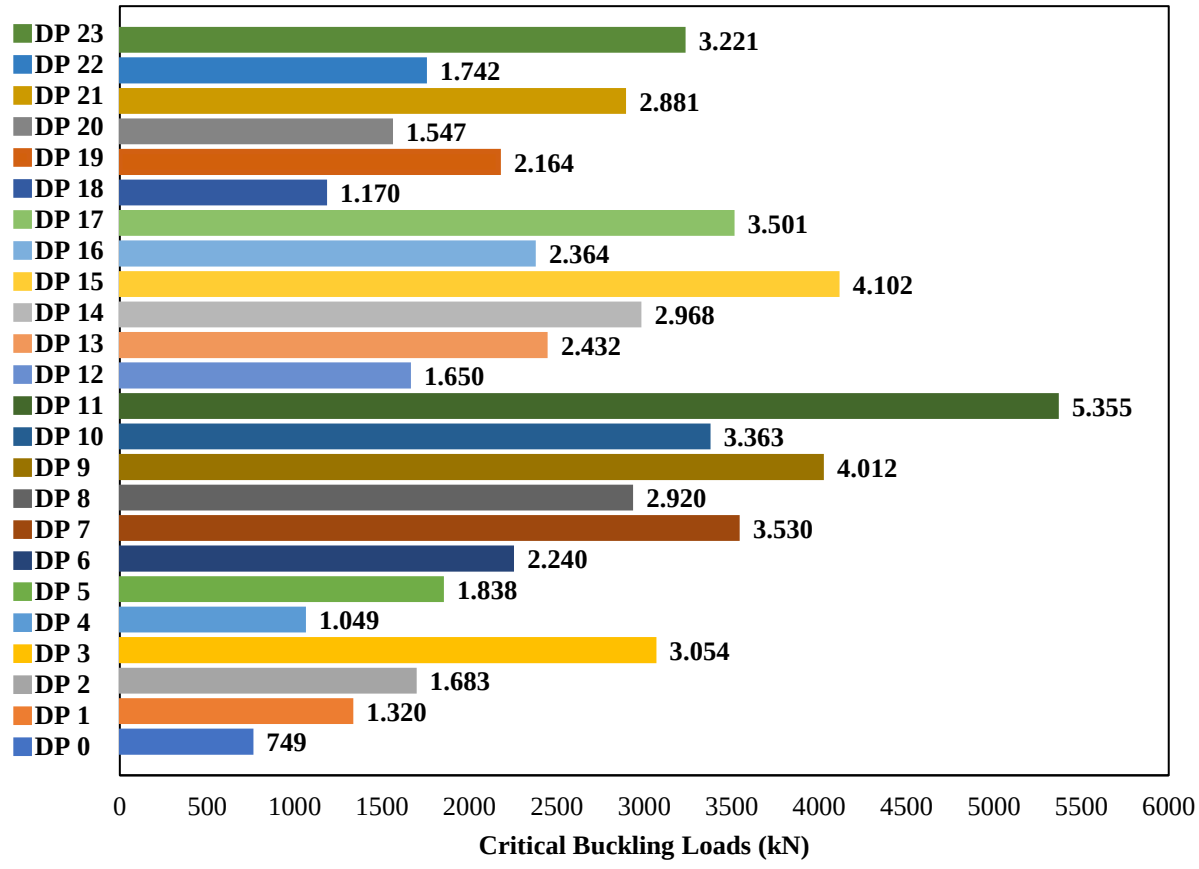


Figure 9. Two first C2 20m pole buckling mode critical loads

Table 6. Critical Buckling Load Comparisons (gains of the second DP with respect to the second)

| Thickness Comparison | Strength gain | Resin Comparison | Strength gain | Fiber Angle Comparison | Strength gain |
|---|---|---|---|---|---|
| DP 0/DP 1 | 69% | DP 0/DP 2 | 128% | DP 0/DP 6 | 184% |
| DP 2/DP 3 | 74% | DP 0/DP 4 | 40% | DP 0/DP 12 | 110% |
| DP 4/DP 5 | 68% | DP 2/DP 4 | -39% | DP 0/DP 18 | 57% |
| DP 6/DP 7 | 50% | DP 6/DP 8 | 34% | DP 6/DP 12 | -26% |
| DP 8/DP 9 | 31% | DP 6/DP 10 | 50% | DP 6/DP 18 | -45% |
| DP 10/DP 11 | 52% | DP 8/DP 10 | 12% | DP 12/DP 18 | -25% |
| DP 12/DP 13 | 40% | DP 12/DP 14 | 84% | DP 2/DP 8 | 67% |
| DP 14/DP 15 | 32% | DP 12/DP 16 | 43% | DP 2/DP 14 | 69% |
| DP 16/DP 17 | 41% | DP 14/DP 16 | -22% | DP 2/DP 20 | -8% |
| DP 18/DP 19 | 77% | DP 18/DP 20 | 34% | DP 8/DP 14 | 2% |
| DP 20/DP 21 | 79% | DP 18/DP 22 | 49% | DP 8/DP 20 | -45% |
| DP 22/DP 23 | 77% | DP 20/DP 22 | 11% | DP 14/DP 20 | -46% |
| | | | | DP 4/DP 10 | 204% |
| | | | | DP 4/DP 16 | 115% |
| | | | | DP 4/DP 22 | 67% |
| | | | | DP 10/DP 16 | -29% |
| | | | | DP 10/DP 22 | -45% |
| | | | | DP 16/DP 22 | -22% |

The highest buckling load was obtained for DP 11, which resulted 537 kN for C1 30m pole and 5,355 kN for C2 20m. DP 11 corresponds to resin C composites, 40 mm of total thickness and 72 layers of ±30° fibers. Given that all configurations, considering same total thickness, present similar moment of inertia, this configuration presented the highest buckling load because of its higher Young's modulus associated to the axial compression loading direction. For this analysis, the optimal fibers orientation was found to be ±30° fibers, which is the closest alignment of the fiber directions to the axial loading, ensuring that the higher Young's modulus has significant contribution on the axial direction.

From Table 6 it is possible to notice that the buckling strength increase is quite different when comparing design points with same resin and fiber orientation, ranging from 31% to 79%. The greatest strength gains were observed for the combined fiber orientations, it can be noted that the combination of different fiber orientations resulted in the elimination of a preferential direction, significantly reducing the impact of the definition of orthotropic properties in the determination of buckling strength.

An average increase of 800% on buckling strength at any design point is observed when comparing C2 20m and C1 30m poles, so its noticeable that the C2 20m pole is more suitable for transmission lines application in general manner, when assuming there is no ground-cable distance restrains.

### 4.2 Non-linear static analysis results

The structural performance of the composite material considering the impact of resin type and fiber considers the nonlinear buckling in terms of stresses, displacements and equilibrium curve. The vertical load versus vertical displacement and the lateral load versus lateral displacement curves shows the mechanical response of the composite structures for all the parameters combinations. This assessment is shown only for C1 30m structure, since this configuration presents greater flexibility, and therefore, its behavior is more influenced by geometric nonlinearities.

### 4.3 Effect of fiber orientation

As observed in Figures Figure 10, Figure 11, Figure 12, Figure 13 and Figure 14, a lower displacement occurs when fibers are oriented at ±30°, for composite materials using both resins A and C. This is explained due the fact that resins A and C have a higher Young's modulus in the direction of the fibers. However, for fibers oriented at ±45°, resin B shows the best structural response, since this composite have similar mechanical behavior for all directions. Additionally, for resin B fibers oriented at ±30° exhibited the second-best mechanical behavior, both of them with 72 layers.

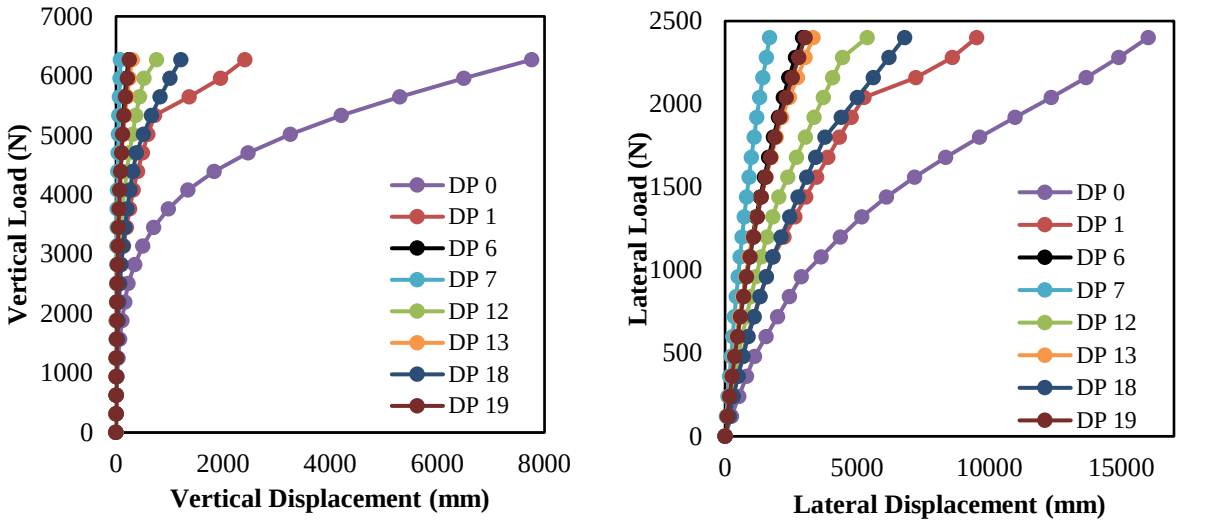


Figure 10. Fiber orientation angle comparison for resin A: load versus displacement curves

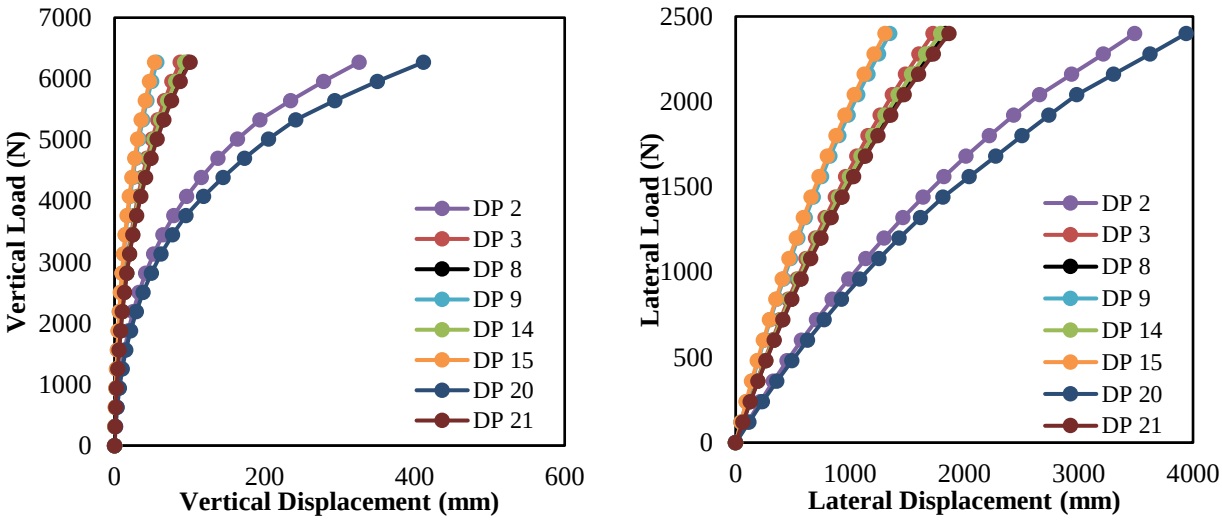


Figure 11. Fiber orientation angle comparison for resin B: load versus displacement curves

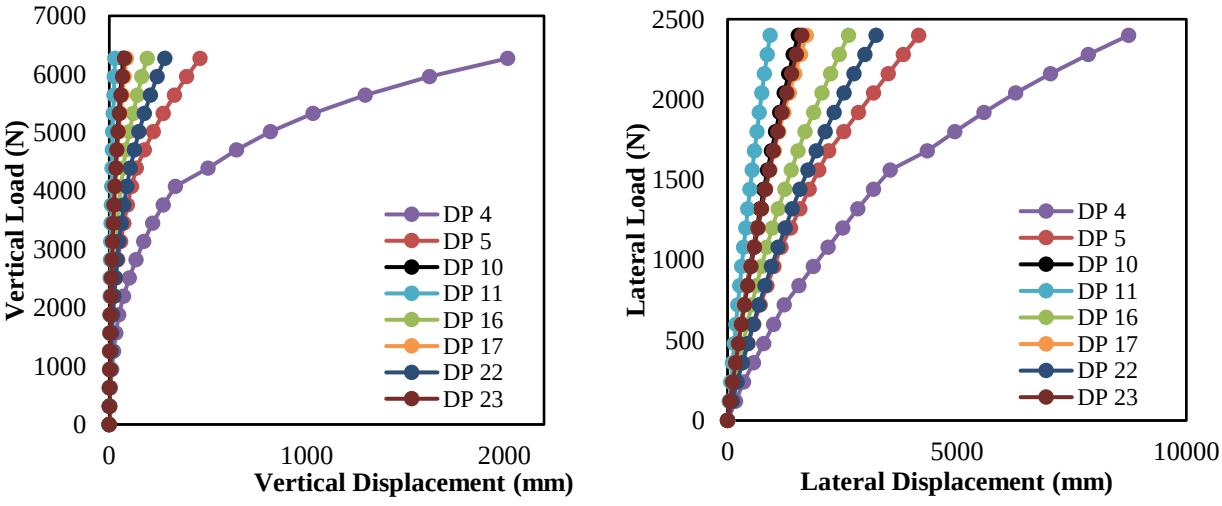


Figure 12. Fiber orientation angle comparison for resin C: load versus displacement curves

### 4.4 Type of resin impact

Figures Figure 10, Figure 11, Figure 12, Figure 13 and Figure 14, it is observed that the composites matrix made of resin type A shows larger displacements than resins B and C. This is verified when comparing any fiber orientation or overall thickness. Additionally, it is noticed that for the cases of fibers oriented at ±60° or ±45°, resin B presented the best structural behavior, whether the composite with a total thickness of 40 mm or 20 mm, the latter still performing better than the other resins with a total thickness of 40 mm for fibers oriented at ±60°. The design point 11, which comprises a composite with a resin C matrix, fibers oriented at ±45° and a total thickness of 40 mm, presented the best behavior from a structural point of view, due to its lower displacement and also lower stresses, developed for the same amount of applied load, which ensures attendance to ultimate limit state and serviceability limit state. This result corroborates the discussion addressed in item 4.1, since this same model also presented the highest critical buckling load.

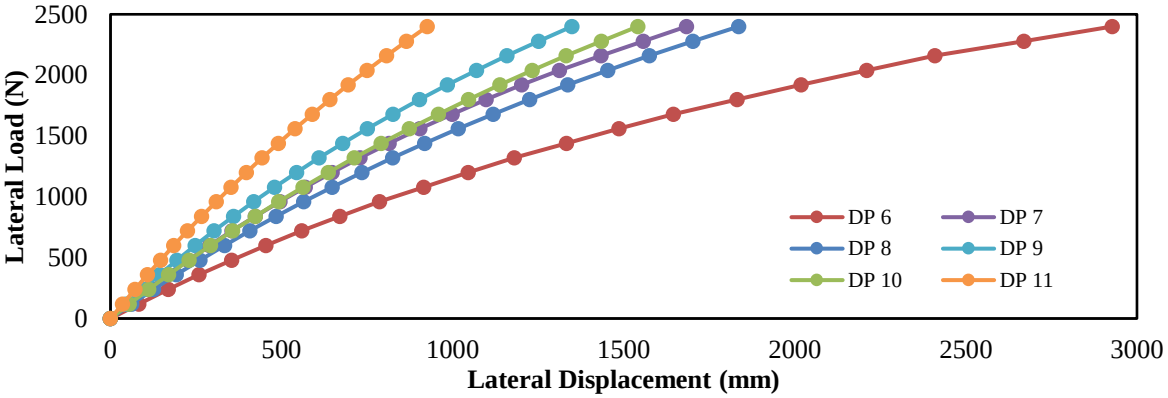


Figure 13. Resin comparison for ±30° fibers: lateral load versus displacement curves

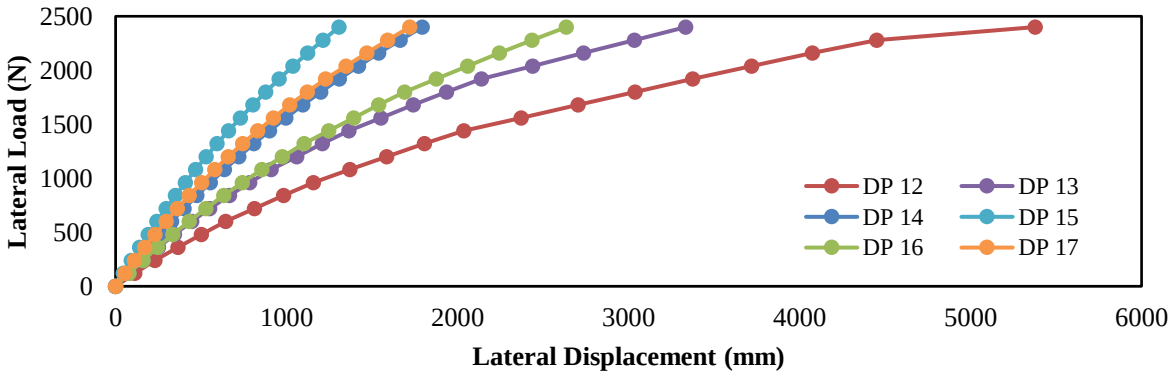


Figure 14. Resin comparison for ±45° fibers: lateral load versus displacement curves

### 4.5 Effect of thickness

By observing DP 6, it could be seen that this configuration presented lower displacements than DP 13, DP 19, and DP 1 which employed the double of thickness, it highlights the effectiveness of employing optimal fiber orientation in composite fabrics. Similar effect occurs when observing DP 8 and DP 14, which performed better than DP 21, a configuration with double of thickness. Finally, it can also be seen that DP 10, presented a stiffer behavior than all other configurations, except the one which employed same fiber orientation and double of thickness.

# 5 Conclusions

This study addresses efforts on comprehending best practices for manufacturing process and design optimization. As the main findings of this paper it could be mentioned that from the structural point of view resin C showed up as the most suitable option, when analyzing the structure equilibrium curves, and also by the critical buckling loads obtained by eigenvalue buckling analysis. The increase of lamina thickness didn't result in a uniform strength gain, when comparing different fiber orientations and resins, since the fiber orientation aspect showed to be predominant, in some situations even when employing double of the composite total thickness. Resin B presented a suitable matrix alternative when employed with fibers at ±45°. Resin A showed up as the most flexible structure, also developing higher stress. Ultimately, when assuming there is no cable-ground restraints C2 poles represents more optimized and stiffer structures.

**Acknowledgements.** The authors gratefully acknowledge support from Copel Geração e Transmissão S.A. (PD-06491-0481/2018 "DESENVOLVIMENTO DE COMPÓSITOS POLIMÉRICOS PARA CONSTRUÇÃO DE TORRES USADAS EM LINHAS DE TRANSMISSÃO").

**Authorship statement.** The authors hereby confirm that they are the sole liable persons responsible for the authorship of this work, and that all material that has been herein included as part of the present paper is either the property (and authorship) of the authors, or has the permission of the owners to be included here.

# References

[1] Marzuki HFA, Jaafar M. Laminate Design of Lightweight Glass Fiber Reinforced Epoxy Composite for Electrical Transmission Structure. Procedia Chem 2016;19:871–8. https://doi.org/10.1016/j.proche.2016.03.128.

[2] Urgessa G, Mohamadi S. Structural Assessment of Fiber-reinforced Polymer Composite Electric Poles. Procedia Eng 2016;145:707–14. https://doi.org/10.1016/j.proeng.2016.04.085.

[3] Ricardo P. COBEM-2017-1383 NUMERICAL ANALYSIS OF GFRP POLES 2017.

[4] ASTM INTERNATIONAL. Standard Test Methods for Flexural Properties of Unreinforced and Reinforced Plastics and Electrical Insulating Materials. 2017. https://doi.org/10.1520/D0790-17.2.

[5] Ansys. Theory Reference Ansys. 2021.